PCCP

PAPER

View Article Online
View Journal | View Issue

Cite this: *Phys. Chem. Chem. Phys.*, 2026, **28**, 6711

Size-dependent femtosecond proton transfer in protonated methanol clusters

Sergei V. Anishchik, [a] Naga Krishnakanth Katturi, [a] Jesse Sandhu [a] and Marcos Dantus *[ab]

Methanol clusters $(CH_3OH)_n$ are prototypical hydrogen-bonded systems that bridge isolated molecules and bulk liquid methanol. Strong-field ionization of these clusters can trigger ultrafast charge migration, proton transfer, and isomerization; however, the onset timescales of these pathways remain largely unexplored despite extensive steady-state mass-spectrometric evidence for protonation and chemical rearrangement. Here we use femtosecond time-resolved strong-field ionization and disruptive probing to directly track the early-time dynamics of methanol clusters. Transient mass spectra yield size-dependent timescales for the formation of protonated clusters $H^+(CH_3OH)_n$ (n = 1–3) and an associated $CHO^{\bullet+}$ radical cation. We find that both proton-transfer and subsequent stabilization become markedly faster with increasing cluster size. These measurements establish methanol clusters as a complementary benchmark to water for understanding ionization-initiated proton motion and chemical reorganization in hydrogen-bonded liquids.

Received 17th December 2025,
Accepted 16th February 2026

DOI: 10.1039/d5cp04925c

rsc.li/pccp

1 Introduction

Hydrogen-bonded clusters of methanol, $(CH_3OH)_n$, provide a versatile model for nano-sized solvent environments whose neutral and protonated ground-state structures are now well characterized over a broad size range. Ionization-induced proton motion in hydrogen-bonded media is a central motif in radiation chemistry and radiation damage, with water serving as the canonical benchmark.[1,2] This relevance extends beyond terrestrial solvation: methanol is widespread in interstellar space and is observed in multiple aggregate states (gas-phase, ices, and mixed molecular environments), where ionizing radiation and secondary electrons can initiate chemistry that likely involves, among other intermediates, ionized methanol clusters.[3–7] Infrared spectroscopy has mapped the evolution of hydrogen-bond motifs in $(CH_3OH)_n$ (n = 2–6) and in larger clusters, revealing cyclic and bicyclic structures and identifying the minimum number of methanol molecules required to stabilize an excess proton.[8–11] In parallel, studies of core- and valence-ionized solvent clusters[12] have demonstrated that ionization-driven proton motion in nano-sized hydrogen-bonded environments is highly sensitive to network strength and confinement, and plays a key role in radiation chemistry, as exemplified by the water dimer.[13,14] In contrast, the time-resolved proton-transfer dynamics of methanol clusters following ionization, and their dependence on cluster size and subsequent relaxation,[15] remain essentially unexplored on the femtosecond timescale. Here we directly measure size-resolved proton-transfer rates in $(CH_3OH)_n$ (n = 2–4) following strong-field ionization, tracking the formation of protonated clusters and CH_3O-containing fragments and identifying a slower picosecond decay of the protonated-cluster yield associated with evaporation and/or structural relaxation.

Extensive theoretical work has been devoted to methanol clusters[16–28] and prior studies have emphasized the importance of proton-transfer processes following cluster ionization, which lead to the formation of protonated cluster ions.[29–31] These protonated clusters remain chemically active, undergoing internal rearrangements and size-dependent fragmentation *en route* to the detector. VUV photoionization studies of the methanol dimer cation established a vertical ionization threshold of 9.7 eV and identified two competing proton-transfer channels: a barrierless hydroxy-proton transfer and a more exothermic methyl-proton transfer that proceeds over a small activation barrier.[31] Near-threshold ionization photoelectron–photoion coincidence (PEPICO) measurements on methanol dimer isotopologues show that protonated methanol arises *via* intracluster proton transfer in the dimer cation, with CH_2OH loss dominating between 10.2–10.5 eV (consistent with methyl-group proton transfer) and $CH_3O\bullet$ loss becoming dominant above 10.6 eV (consistent with hydroxy-proton transfer).[30] The hydrogen transfer process was studied in excited methanol and methanol-water clusters, with a subpicosecond time resolution.[32] However, the

[a] *Department of Chemistry, Michigan State University, East Lansing, MI 48824, United State*
[b] *Department of Physics and Astronomy, Michigan State University, East Lansing, MI 48824, United State. E-mail: dantus@msu.edu*

exact timescales for proton transfer and protonated-cluster formation dynamics have not yet been experimentally determined with femtosecond time resolution. The goal of this study is to observe the time evolution of cluster ion yields using a pump–probe method in the femtosecond time domain.

2 Experimental

Methanol clusters were generated by supersonic expansion of a methanol/argon gas mixture into vacuum through a 10 μm continuous-flow nozzle. The resulting molecular beam was collimated by two skimmers (3 and 4 mm diameter) positioned 10 mm and 22 cm downstream. The base pressure in the interaction chamber was $\sim 1 \times 10^{-9}$ Torr and rose to $\sim 2 \times 10^{-7}$ Torr during data acquisition. Cluster strong-field ionization and detection were carried out in a Wiley–McLaren time-of-flight (TOF) mass spectrometer.

A Ti:sapphire laser (800 nm) delivered 40 fs pulses at 1 kHz. Disruptive probing measurements were performed at both 800/800 nm and 1300/1300 nm, with *in situ* pulse durations at the sample of ~50 fs in each case. The 1300 nm pulses were generated by an optical parametric amplifier pumped by the 800 nm fundamental. The peak intensity at the molecular beam was calibrated using the measured ion-yield ratio of Ar^{2+} to Ar^{+} from the argon carrier gas, following established strong-field intensity calibration procedures.[33] For the 800 nm experiments, the pump/ionization pulse peak intensity at the interaction region was $\sim 6 \times 10^{14}$ W cm^{-2}, and the disruptive probe intensity was $\sim 0.6 \times 10^{14}$ W cm^{-2}. For the 1300 nm measurements, the corresponding peak intensities were $\sim 2 \times 10^{14}$ W cm^{-2} (pump/ionization) and $\sim 0.2 \times 10^{14}$ W cm^{-2} (probe). In both strong-field ionization cases, the Keldysh parameter was $\gamma < 0.4$. In its semiclassical interpretation, γ compares the characteristic tunneling (ionization) time to the optical period; thus $\gamma \ll 1$ implies that ionization occurs within a fraction of a laser cycle. These values place our measurements firmly in the tunneling/field-ionization regime, where ionization is nonperturbative and electron recollision dynamics can contribute, rather than in the perturbative multiphoton regime.[34]

Ion detection employed a multichannel-plate detector and time-resolved mass spectra were recorded by a fast digitizer, averaging $\sim 10^6$ laser shots per delay step to achieve high signal-to-noise. All acquisition conditions were held constant across the entire study, including detector voltage, digitizer sensitivity, and the ion-yield scaling, so signal amplitudes can be compared directly between measurements at different wavelengths.

3 Results

Experimental mass spectra resulting from strong-field ionization at 1300 nm and 800 nm wavelengths are shown in Fig. 1, where the horizontal axis gives the mass-to-charge ratio (m/q) and the vertical axis shows ion yields averaged over $\sim 10^6$ laser shots. In both cases the average laser power was ~170 mW.

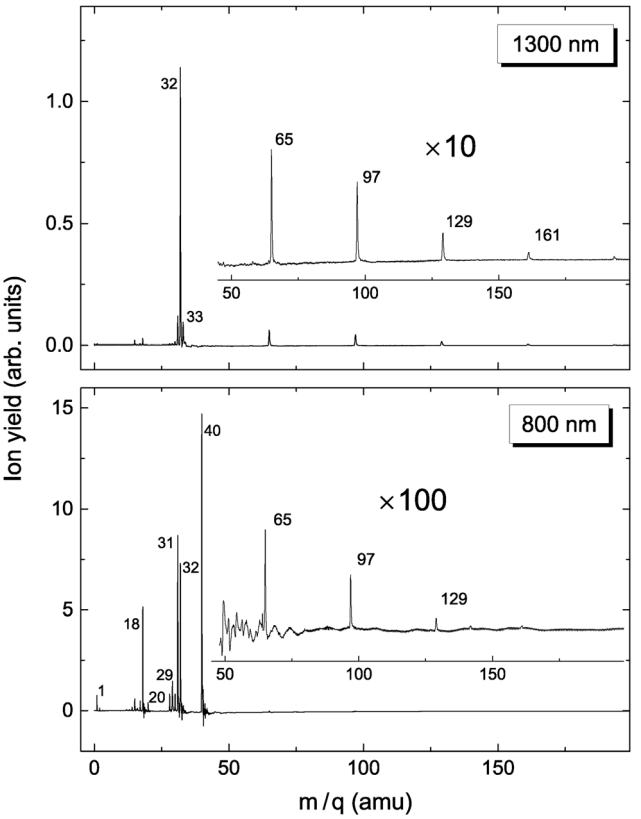

Fig. 1 TOF mass spectra of protonated methanol clusters obtained by strong-field ionization with 1300 nm (top) and 800 nm (bottom) femtosecond pulses. Insets show magnified views of the cluster regions; the masses of the protonated clusters are indicated next to the corresponding peaks. A slight detector ringing artifact is visible in the 800 nm spectrum due to the strong molecular ion signal.

At 1300 nm, the dominant peak appears at m/q 32, assigned to CH_3OH^+, and the spectrum shows additional peaks due to methanol cluster ions. As highlighted in the inset (×10 magnification), these cluster peaks occur at m/q 65, 97, 129, *etc.*, corresponding to protonated clusters $H^+(CH_3OH)_n$ ($n \geq 2$), along with a protonated monomer peak at m/q 33. We observed a very weak line of the unprotonated methanol dimer cation (m/q 64), which had an ion yield over than one order of magnitude weaker than that of any observed protonated cluster. No other lines of unprotonated clusters were observed.

In contrast, the 800 nm spectrum is markedly different. The most intense peak is at m/q 40 (Ar^+), with a weaker Ar^{2+} peak at m/q 20, followed by an intense CH_3O^+ (m/q 31), CH_3OH^+, and a prominent H_2O^+ peak at m/q 18. When the 800 nm spectrum is normalized to its most intense line, cluster ion peaks are barely visible and require ×100 magnification in the inset to be resolved. However, because the absolute ion yield of the most intense 800 nm peak is roughly ten times higher than that of the most intense 1300 nm peak, the absolute ion yields of the methanol clusters for the two wavelengths are in fact comparable.

Fig. 2 shows the measurement results at different gas pressures in the nozzle. All experiments were carried out using a laser with a wavelength of 1300 nm. The top figure (Fig. 2a)

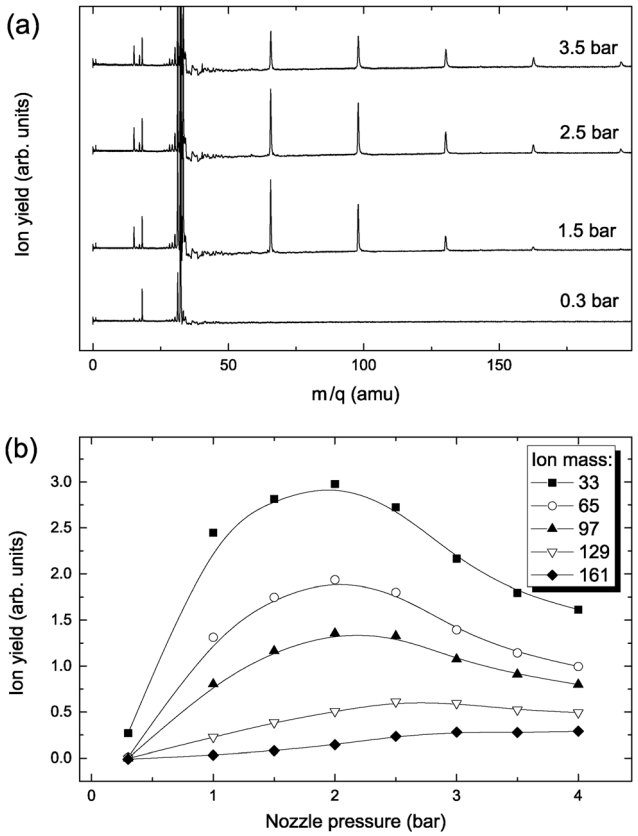

Fig. 2 (a) Mass spectra of methanol clusters recorded with a 1300 nm pump laser at different nozzle stagnation pressures. All spectra are plotted on the same intensity scale and vertically offset for clarity; the corresponding pressures (in bar) are indicated next to each trace. (b) Ion yields as a function of nozzle pressure for protonated methanol ($H^+(CH_3OH)$, m/q 33) and protonated methanol clusters ($H^+(H_3OH)_n$, $m/q = 32n + 1$, $n = 2$–5). Data points are connected by spline curves as a guide to the eye.

shows the mass spectra at nozzle pressures of 0.3, 1.5, 2.5, and 3.5 bar. All spectra are shown in the same scale, allowing the lines of protonated clusters to be clearly seen. As can be seen from the figure, at a pressure of 0.3 bar, clusters are not observed at all, but as the pressure increases, lines of increasingly heavier clusters appear.

In the bottom figure (Fig. 2b) we can see the dependence of integrated intensity of the spectral lines of protonated methanol (m/q = 33) and protonated clusters $H^+(CH_3OH)_n$ (m/q = 65, 97 129, and 161, at $n = 2 - 5$) on the nozzle pressure. Fig. 2(b) shows that with increasing pressure, the yield of ions from clusters initially increases and then begins to fall as increasingly larger clusters are formed. This is explained by the fact that in the pressure range we use, the efficiency of adiabatic cooling during supersonic expansion into a vacuum increases with increasing the nozzle pressure. As a result, increasingly larger clusters are formed. All further experiments were carried out at a nozzle pressure of 2 bar, since at this pressure the highest intensity of the lines of protonated methanol dimers and trimers was observed.

The pump–probe delay dependence of the ion yield was measured by integrating the corresponding peak in the mass

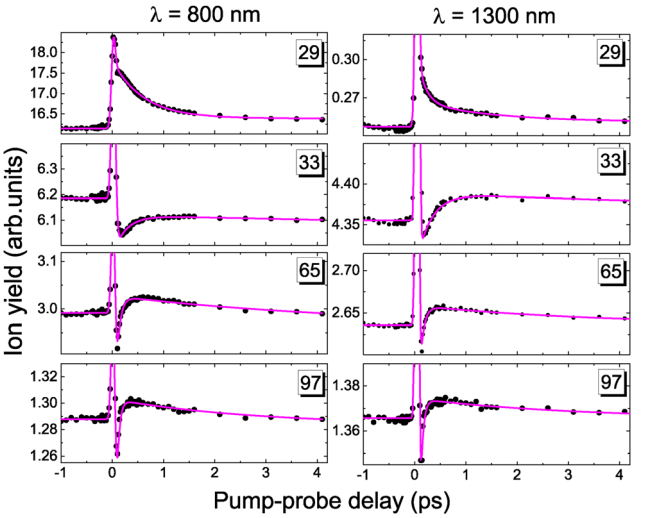

Fig. 3 Pump–probe delay dependence of the ion yields for m/q 29 (HCO^+), 33 (H^+CH_3OH), 65 ($H^+(CH_3OH)_2$), and 97 ($H^+(CH_3OH)_3$) at 800 nm (left column) and 1300 nm (right column). Closed circles show the experimental data (integrated peak areas); solid lines are fits according to eqn (1). For each ion, the transients recorded at the two wavelengths are very similar.

spectrum and averaging over $\sim 10^6$ laser shots. The resulting data, shown as closed circles in Fig. 3, are plotted for m/q 29 (assigned to HCO^+), m/q 33 (H^+CH_3OH), m/q 65 ($H^+(CH_3OH)_2$), and m/q 97 ($H^+(CH_3OH)_3$). For each ion, including the protonated methanol monomer, dimer, and trimer, the transients recorded at 800 and 1300 nm are very similar, indicating that the underlying dynamics are largely insensitive to the excitation wavelength in this range. Protonated methanol and its dimer and trimer exhibit similar ion-yield transients: a sharp initial decrease, followed by a rapid recovery and then a gradual decay. In contrast, the m/q 29 signal shows a distinctly different behavior, with an initial increase after excitation and a subsequent monotonic decrease. The solid lines in Fig. 3 are fits using eqn (1), which describes the time-resolved ion yield under irradiation by a Gaussian laser pulse.[34] The extracted time constants t_1 and t_2 from this bi-exponential fit are summarized in Table 1.

$$I(t) = C + A_g \exp\left(-\frac{(t-t_0)^2}{s^2}\right) + \sum_{i=1}^{N} a_i \exp\left(-\frac{(t-t_0)}{t_i}\right)\left[1 + \mathrm{erf}\left(\frac{t-t_0}{s} - \frac{s}{2t_i}\right)\right]. \quad (1)$$

Table 1 The characteristic times t_1 and t_2, were obtained by fitting the experimental time-resolved ion yields to eqn (1) using the two-exponential approximation

Ion	Ion mass (amu)	800 nm t_1 (fs)	800 nm t_2 (fs)	1300 nm t_1 (fs)	1300 nm t_2 (fs)
$H^+(CH_3OH)$	33	260 ± 50	3140 ± 1300	230 ± 30	3500 ± 870
$H^+(CH_3OH)_2$	65	103 ± 10	1450 ± 280	81 ± 15	2300 ± 350
$H^+(CH_3OH)_3$	97	59 ± 10	1410 ± 160	60 ± 15	1400 ± 500

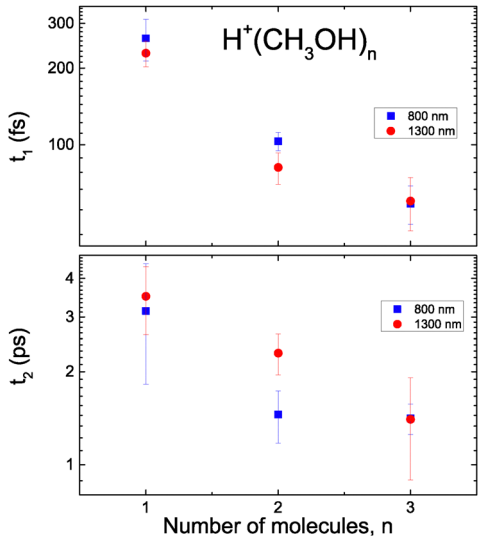

Fig. 4 Dependence of rise times t_1 (top) and fall times t_2 (bottom) on the size of the protonated methanol clusters for wavelengths of 800 nm and 1300 nm.

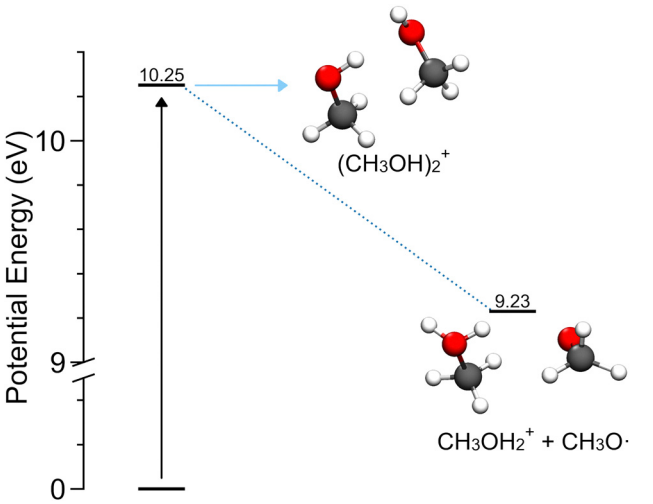

Fig. 5 Reaction coordinate diagram of the proton transfer after vertical ionization of the neutral dimer $(CH_3OH)_2$. The geometries and energies were calculated using B3LYP/def2-TZVP. After vertical ionization, the hydrogen atom attached to oxygen migrates over to the other oxygen, forming $CH_3OH_2^+ + CH_3O\bullet$.

The extracted fast rise (t_1) and slow decay (t_2) time components are summarized in Fig. 4. The horizontal axis gives the cluster size, and the vertical axis shows t_1 and t_2 on a logarithmic scale. As the cluster size increases, the fast component t_1 decreases by approximately a factor of five, while the slow component t_2 decreases by about a factor of about three.

4 Discussion

The observed time-resolved ion yields can be rationalized as follows. The probe pulse alone is not energetic enough to ionize the molecules, but in combination with the pump pulse it can affect the ion yield. The sharp peak at zero delay arises from the temporal overlap of pump and probe, which effectively adds their intensities and thus enhances ionization. Immediately after ionization the ions are far from equilibrium, and the influence of the probe pulse is strongest. Different ions respond to this additional excitation in different ways. For the HCO^+ ion (m/q 29), a fragment of the methanol ion, the probe pulse leads to a pronounced increase in yield, indicating an enhancement of this dissociation channel (see Fig. 3). In contrast, for methanol clusters we observe a sharp decrease in the ion yields, suggesting that the probe pulse induces fragmentation of the far from equilibrium cluster ions.

$$(CH_3OH)_n^+ \rightarrow H^+(CH_3OH)_{n-1} + CH_3O, \qquad (2)$$

After the rapid initial relaxation of the excitation energy, the probe pulse predominantly perturbs the system by interrupting the ongoing evolution of the ions at a given delay time, thereby allowing us to map out their natural dynamics.[34] It is reasonable to attribute the subsequent rapid rise of the protonated methanol and methanol cluster signals to the proton-transfer reaction which should proceed with near-unit probability, as only protonated clusters are observed. We simulated the evolution of the methanol dimer following vertical ionization using *ab initio* molecular dynamics (AIMD) to elucidate the mechanism of proton transfer in methanol clusters. Owing to computational cost, we restricted the AIMD analysis to the dimer. Fig. 5 presents the reaction-coordinate diagram for the proton-transfer process, and a representative reactive trajectory is provided as a movie in the SI. Computational details are given in Appendix A.

Previous threshold-photoionization studies of $(CD_3OH)_2^+$ indicate that hydroxy-proton transfer is essentially barrierless near onset, whereas methyl-proton transfer is slower and consistent with a modest rearrangement barrier.[31] In the present strong-field ionization measurements, the dimer cation is formed with excess internal energy, and the observed ultrafast dynamics therefore reflect proton transfer and early relaxation above the appearance thresholds, where both channels may be accessible. Because our measurements were performed on methanol (CH_3OH), the product ions do not uniquely tag the origin of the transferred proton, and we cannot separate hydroxy- *versus* methyl-derived proton transfer from the mass spectra alone. Disentangling these pathways will require isotope-labeling experiments using partially deuterated methanol (*e.g.*, CH_3OD and/or CD_3OH) to provide unambiguous mass signatures for the competing channels.

In our calculations, a transition-state search along the hydroxyl-group proton-transfer coordinate did not locate any barrier (*i.e.*, no corresponding transition-state structure was found), indicating a barrierless pathway. This result is consistent with previous theoretical and experimental studies on methanol dimers,[31] as well as with analogous findings reported for the formic acid dimer.[35]

As the cluster size increases, the number of possible proton-transfer pathways grows, leading to a decrease in the characteristic time of this process. The slower decay of the ion yields at

longer delays is associated with further reactions of the protonated clusters, the simplest of which is the loss of a neutral molecule,

$$H^+(CH_3OH)_n \rightarrow H^+(CH_3OH)_{n-1} + CH_3OH. \quad (3)$$

From these measurements we draw several conclusions regarding methanol cluster formation and dynamics. First, methanol clusters are reliably detected following strong-field ionization and are observed exclusively in protonated form. Second, in contrast to most other mass-spectral features of the monomer, the yield of protonated cluster ions depends only weakly on the laser wavelength. Third, the time-dependent ion yields of protonated methanol and its protonated clusters in the pump–probe experiment exhibit similar behavior, characterized by an initial rapid rise followed by a much slower decay. Finally, the corresponding rise (t_1) and decay (t_2) time constants show only a weak dependence on wavelength but decrease systematically with increasing cluster size.

The femtosecond protonation dynamics that we observe in methanol clusters can be placed in the broader context of ultrafast proton transfer in hydrogen-bonded systems. Schnorr and co-workers have recently shown that, upon ionization, the water dimer radical cation undergoes proton transfer on a time scale of $\sim$55 fs, as directly tracked by XUV pump–probe ion-coincidence spectroscopy that detects delay-dependent H_3O^+ + OH^+ pairs and the associated structural rearrangement of the dimer cation.[13] In our case, the rapid rise of the protonated methanol and cluster signals, characterized by the time constant t_1, likewise occurs on the femtosecond scale, shows only a weak dependence on excitation wavelength, and becomes faster with increasing cluster size. Together, these results suggest that once a radical cation is created, proton transfer along an O–H$\cdots$O hydrogen bond proceeds in an essentially barrierless fashion in both water and methanol aggregates, with additional molecules reducing the timescale. The slower decay component t_2 that we extract for methanol clusters can then be interpreted as structural relaxation of the cluster, emphasizing the generality of ultrafast proton migration followed by slower reorganization in ionized hydrogen-bonded networks.

The size-dependent femtosecond proton-transfer kinetics and picosecond relaxation we observe in ionized methanol clusters provide a quantitative link between established structural pictures of neutral and protonated methanol networks and their nonequilibrium dynamics after ionization. Our results show that as few as two methanol molecules are needed to efficiently accept and delocalize a proton, provide benchmark time scales and product branching ratios (protonated cluster *vs.* CH_3O• formation) for testing nonadiabatic electronic-structure and dynamics methods, and constrain models of energy flow and evaporation in nano-sized hydrogen-bonded droplets. Beyond methanol, these data inform the description of hydrogen-bond network strength in confined geometries, the early steps of radiation chemistry in protic organic liquids, and proton transport in microsolvated environments relevant to atmospheric and astrochemical nanoices. By positioning methanol clusters alongside water dimers and mixed solvent clusters as a new dynamical benchmark, this work opens a route to systematically compare ionization-induced proton motion across different hydrogen-bonded liquids.

Author contributions

S. V. Anishchik: conceptualization, methodology, software, validation, formal analysis, investigation, data curation, writing – original draft, writing – review & editing, visualization. N. Krishnakanth Katturi: methodology, software, validation, formal analysis, investigation, writing – original draft, writing – review & editing. J. Sandhu: the molecular dynamic simulation, writing – original draft, writing – review & editing, visualization. M. Dantus: conceptualization, methodology, validation, formal analysis, investigation, resources, data curation, writing – review & editing, visualization, supervision, project administration, funding acquisition.

Conflicts of interest

The authors declare no competing interests.

Data availability

All data needed to evaluate the conclusions of this study are included in the article. Any additional information related to this study may be requested from the authors.

Supplementary information (SI) is available and includes a movie of a representative AIMD trajectory showing proton transfer in the ionized methnol dimer. See DOI: https://doi.org/10.1039/d5cp04925c.

Appendix

Appendix A. Computational details

To gain additional insight into proton transfer in ionized $(CH_3OH)_n$ clusters, we performed *ab initio* molecular dynamic (AIMD) simulations with the ORCA computational chemistry package.[36] In total, 22 trajectories were propagated at the B3LYP/def2-TZVP level using a 0.5 fs time-step and a total simulation time of 2 ps per trajectory. Ionization was modeled as a vertical transition from the neutral ground state to the cationic ground state; accordingly, each trajectory was initialized from the optimized neutral equilibrium geometry computed at the same level of theory. Initial velocities were assigned by sampling a Maxwell–Boltzmann distribution. Owing to computational cost, AIMD was performed only for the dimer. The computed vertical ionization energy is in good agreement with prior theoretical work[29] and with available experimental results.[37]

Of the 22 trajectories, one exhibited proton transfer, four remained nonreactive over the full 2 ps, and the remainder separated without undergoing proton transfer. In the reactive trajectory, the hydrogen involved in the intermolecular hydrogen

bond is the proton that transfers, and the transfer completes within ~50 fs.

Acknowledgements

This material is based upon work supported by the U.S. Department of Energy, Office of Science, Office of Basic Energy Sciences, Chemical Sciences, Geosciences, and Biosciences Division, Gas Phase Chemical Physics Program, under Award Number DE-SC0025576. Disclaimer: This report was prepared as an account of work sponsored by an agency of the United States Government. Neither the United States Government nor any agency thereof, nor any of their employees, makes any warranty, express or implied, or assumes any legal liability or responsibility for the accuracy, completeness, or usefulness of any information, apparatus, product, or process disclosed, or represents that its use would not infringe privately owned rights. Reference herein to any specific commercial product, process, or service by trade name, trademark, manufacturer, or otherwise does not necessarily constitute or imply its endorsement, recommendation, or favoring by the United States Government or any agency thereof. The views and opinions of authors expressed herein do not necessarily state or reflect those of the United States Government or any agency thereof.

References

1 J. Ward, in *Progress in Nucleic Acid Research and Molecular Biology*, ed. W. E. Cohn and K. Moldave, Academic Press, 1988, vol. 35, pp. 95–125.
2 G. V. Buxton, C. L. Greenstock, W. P. Helman and A. B. Ross, *J. Phys. Chem. Ref. Data*, 1988, **17**, 513–886.
3 P. Friberg, S. C. Madden, A. Hjalmarson and W. M. Irvine, *Astron. Astrophys.*, 1988, **195**, 281–289.
4 E. Dartois, W. Schutte, T. R. Geballe, K. Demyk, P. Ehrenfreund and L. D'Hendecourt, *Astron. Astrophys.*, 1999, **342**, L32–L35.
5 E. S. Wirström, W. D. Geppert, Å. Hjalmarson, C. M. Persson, J. H. Black, P. Bergman, T. J. Millar, M. Hamberg and E. Vigren, *Astron. Astrophys.*, 2011, **533**, A24.
6 A. A. Boogert, P. A. Gerakines and D. C. Whittet, *Annu. Rev. Astron. Astrophys.*, 2015, **53**, 541–581.
7 C. Walsh, R. A. Loomis, K. I. Öberg, M. Kama, M. L. R. van't Hoff, T. J. Millar, Y. Aikawa, E. Herbst, S. L. Widicus Weaver and H. Nomura, *Astrophys. J., Lett.*, 2016, **823**, L10.
8 Y. J. Hu, H. B. Fu and E. R. Bernstein, *J. Chem. Phys.*, 2006, **125**, 154306.
9 A. Fujii, S. Enomoto, M. Miyazaki and N. Mikami, *J. Phys. Chem. A*, 2005, **109**, 138–141.
10 T. Shimamori, J.-L. Kuo and A. Fujii, *J. Phys. Chem. A*, 2016, **120**, 9203–9208.
11 T. Kobayashi, R. Shishido, K. Mizuse, A. Fujii and J.-L. Kuo, *Phys. Chem. Chem. Phys.*, 2013, **15**, 9523–9530.
12 Z. Lyu, G. Hallett-Tapley and G. Orlova, *Comput. Theor. Chem.*, 2020, **1171**, 112661.
13 K. Schnorr, M. Belina, S. Augustin, H. Lindenblatt, Y. Liu, S. Meister, T. Pfeifer, G. Schmid, R. Treusch, F. Trost, P. Slavícek and R. Moshammer, *Sci. Adv.*, 2023, **9**, eadg7864.
14 M. Johny, C. A. Schouder, A. Al-Refaie, L. He, J. Wiese, H. Stapelfeldt, S. Trippel and J. Küpper, *Phys. Chem. Chem. Phys.*, 2024, **26**, 13118–13130.
15 P.-J. Hsu, A. Mizuide, J.-L. Kuo and A. Fujii, *Phys. Chem. Chem. Phys.*, 2025, **27**, 18430–18443.
16 J. E. D. Bene, *J. Chem. Phys.*, 1971, **55**, 4633–4636.
17 W. L. Jorgensen, *J. Chem. Phys.*, 1979, **71**, 5034–5038.
18 O. Mó, M. Yáñez and J. Elguero, *J. Chem. Phys.*, 1997, **107**, 3592–3601.
19 U. Buck, J.-G. Siebers and R. J. Wheatley, *J. Chem. Phys.*, 1998, **108**, 20–32.
20 R. D. Parra and X. C. Zeng, *J. Chem. Phys.*, 1999, **110**, 6329–6338.
21 G. S. Tschumper, J. M. Gonzales, I. Schaefer and F. Henry, *J. Chem. Phys.*, 1999, **111**, 3027–3034.
22 J. David, D. Guerra and A. Restrepo, *J. Phys. Chem. A*, 2009, **113**, 10167–10173.
23 M. M. Pires and V. F. DeTuri, *J. Chem. Theory Comput.*, 2007, **3**, 1073–1082.
24 S. L. Boyd and R. J. Boyd, *J. Chem. Theory Comput.*, 2007, **3**, 54–61.
25 J. J. Fifen, M. Nsangou, Z. Dhaouadi, O. Motapon and N.-E. Jaidane, *J. Chem. Phys.*, 2013, **138**, 184301.
26 S. Kazachenko, S. Bulusu and A. J. Thakkar, *J. Chem. Phys.*, 2013, **138**, 224303.
27 S. R. Gadre, S. D. Yeole and N. Sahu, *Chem. Rev.*, 2014, **385**, 12132–12173.
28 A. Samuilov and Y. Samuilov, *New J. Chem.*, 2023, **47**, 18027–18038.
29 H. Tachikawa, *Chem. Phys.*, 1999, **244**, 263–272.
30 X. Wu, X. Zhou, S. Bjelić, P. Hemberger, B. Sztáray and A. Bodi, *Phys. Chem. Chem. Phys.*, 2022, **24**, 1437–1446.
31 S. Martrenchard, G. Grégoire, C. Dedonder-Lardeux, C. Jouvet and D. Solgadi, *PhysChemComm*, 1999, **2**, 15–19.
32 E. S. Wisniewski, M. A. Hershberger and A. W. Castleman Jr., *J. Chem. Phys.*, 2002, **116**, 5738–5745.
33 T. Weber, M. Weckenbrock, A. Staudte, L. Spielberger, O. Jagutzki, V. Mergel, F. Afaneh, G. Urbasch, M. Vollmer, H. Giessen and R. Dörner, *J. Phys. B: At., Mol. Opt. Phys.*, 2000, **33**, L127.
34 B. Jochim, L. DeJesus and M. Dantus, *Rev. Sci. Instrum.*, 2022, **93**, 033003.
35 S. Barik, E. Livshits, R. Baer and D. Strasser, *J. Phys. Chem. A*, 2025, **129**, 7768–7774.
36 F. Neese, *Wiley Interdiscip. Rev.: Comput. Mol. Sci.*, 2025, **15**, e70019.
37 S. Tomoda and K. Kimura, *Chem. Phys.*, 1983, **74**, 121–126.

